Applied Catalysis B: Environmental 255 (2019) 117738

Contents lists available at ScienceDirect

Applied Catalysis B: Environmental

journal homepage: www.elsevier.com/locate/apcatb

Al-ZnO/CdS Photoanode Modified with a Triple Functions Conformal TiO_2 Film for Enhanced Photoelectrochemical Efficiency and Stability

Ruyi Wang[a,c], Lu Wang[a,c], Yong Zhou[a,b,c,e,*], Zhigang Zou[a,c,d,e]

[a] National Laboratory of Solid State Microstructures, Collaborative Innovation Center of Advanced Microstructures, Department of Physics, Eco-materials and Renewable Energy Research Center (ERERC), Nanjing University, Nanjing 210093, PR China
[b] State Key Laboratory of Environmental Friendly Energy Materials, Southwest University of Science and Technology, Mianyang, Sichuan 621010, PR China
[c] Jiangsu Provincial Key Laboratory of Nanotechnology, PR China
[d] College of Engineering and Applied Science, Nanjing University, Nanjing 210093, PR China
[e] KunshanSunlaite New Energy Co. Ltd., Kunshan Innovation Institute of Nanjing University, Kunshan, No. 1666, South Zuchongzhi Road, Jiangsu 215347, PR China

ARTICLE INFO

Keywords:
Al-ZnO/CdS
TiO_2 passivation layer
photostability
photoelectrichemical

ABSTRACT

ZnO/ CdS based nanorod arrays is an excellent class of photoanode materials with high photoelectric response. However, the poor photostability of CdS in aqueous solution seriously prevents its practical application. Although efforts have been made, it still challengeable to improve stability while maintaining initial photocurrent. Herein, a highly efficient photoanode system consisting of Al-doped ZnO nanorod arrays (NRs) served as effective electron-transfer layer and CdS as a light harvesting layer was designed. At last, TiO_2 protective layer was deposited onto Al-ZnO/CdS photoanodes through atomic layer deposition (ALD) to enhance the photostability. The integrated Al-ZnO/CdS/TiO_2 photoanode exhibits a photocurrent of 11.7 mA/cm^2 at 1.23 V versus reversible hydrogen potential (RHE) and conversion efficiency of 5.9 % at 0.48 V versus RHE for 60 ALD TiO_2 cycles. More importantly, the photostability of Al-ZnO/CdS/TiO_2 photoanode was significantly prolonged comparing with the untreated Al-ZnO/CdS photoanode. The strengthen stability is benefited from the triple functions of ALD TiO_2 layer, that is, isolating the direct contact between the photoanode with the surrounding liquid environment, passivating the surface state of the CdS, and capturing as well as storing the photogenerated hole.

1. Introduction

Photoelectrochemical (PEC) water splitting using semiconductor photoelectrodes offers a promising route to ease the dependence on fossil fuel and contribute to resolve the global warming issue [1–4]. As the performance of photoelectrodes used for solar water splitting continues to improve, enhancement of the long-term stability of the photoelectrodes becomes an increasingly crucial issue to meet the demand for plant-scale operation [5,6]. Among various materials, cadmium sulphide (CdS) is regarded as one of the most promising candidates due to its appropriate bandgap (2.2-2.4 eV) and suitable band-edge positions [7–10]. However, the use of CdS is still hindered by its fast recombination of photoexcited charge carriers and poor stability in aqueous solution upon light illumination [11–13]. Coupling of CdS with another semiconductor, such as ZnO nanorod arrays (NRs) to form ZnO/CdS heterojunction, could generate an interface electric field by band-edge offset, which can effectively accelerate the separation and transfer of photogenerated carriers [14–22]. Thank to highly effective solar energy absorption of CdS and excellent electrical transport property of ZnO NRs, the CdS modified ZnO NRs exhibit superior PEC properties. However, the poor stability of CdS in aqueous solution upon light illumination makes it still a challenge to obtain an efficient ZnO/CdS photoanode with a superior photostability simultaneously [23–28].

Very recently, passivating over-layer, especially TiO_2, has been used to improve the PEC stability of Si [28–30], GaAs [31], GaP [32], and $GaInP_2$ [33]. Thin protective layer can passivate surface charge recombination by preventing formation of the surface defect states and protect photoelectrodes from chemical corrosion around ambient electrolyte environment [34]. Studies have shown that the effect of the passivation layer on the profermance of photoelectrodes is dependent on the substrate material. A very thin layer (often only 1-2 nm) on the photoelectrodes can alter the surface properties [30]. In addition, usually existing an optimal thickness, thin enough to allow interfacial charge transfer and thick enough to provide chemical resistance to the

* Corresponding author at: National Laboratory of Solid State Microstructures, Collaborative Innovation Center of Advanced Microstructures, Department of Physics, Eco-materials and Renewable Energy Research Center (ERERC), Nanjing University, Nanjing 210093, PR China.
E-mail address: zhouyong1999@nju.edu.cn (Y. Zhou).

https://doi.org/10.1016/j.apcatb.2019.05.040
Received 26 February 2019; Received in revised form 30 April 2019; Accepted 11 May 2019
Available online 14 May 2019
0926-3373/

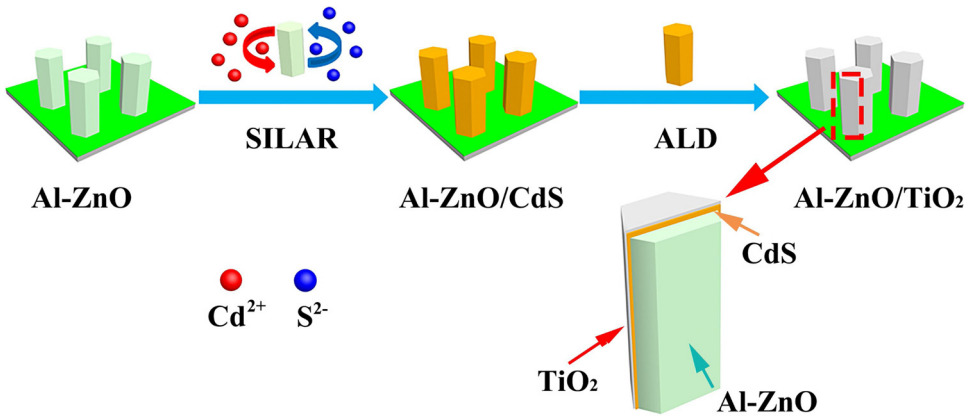

Fig. 1. Schematic diagram of the main process for the fabrication of Al-ZnO/CdS/TiO_2 photoanode.

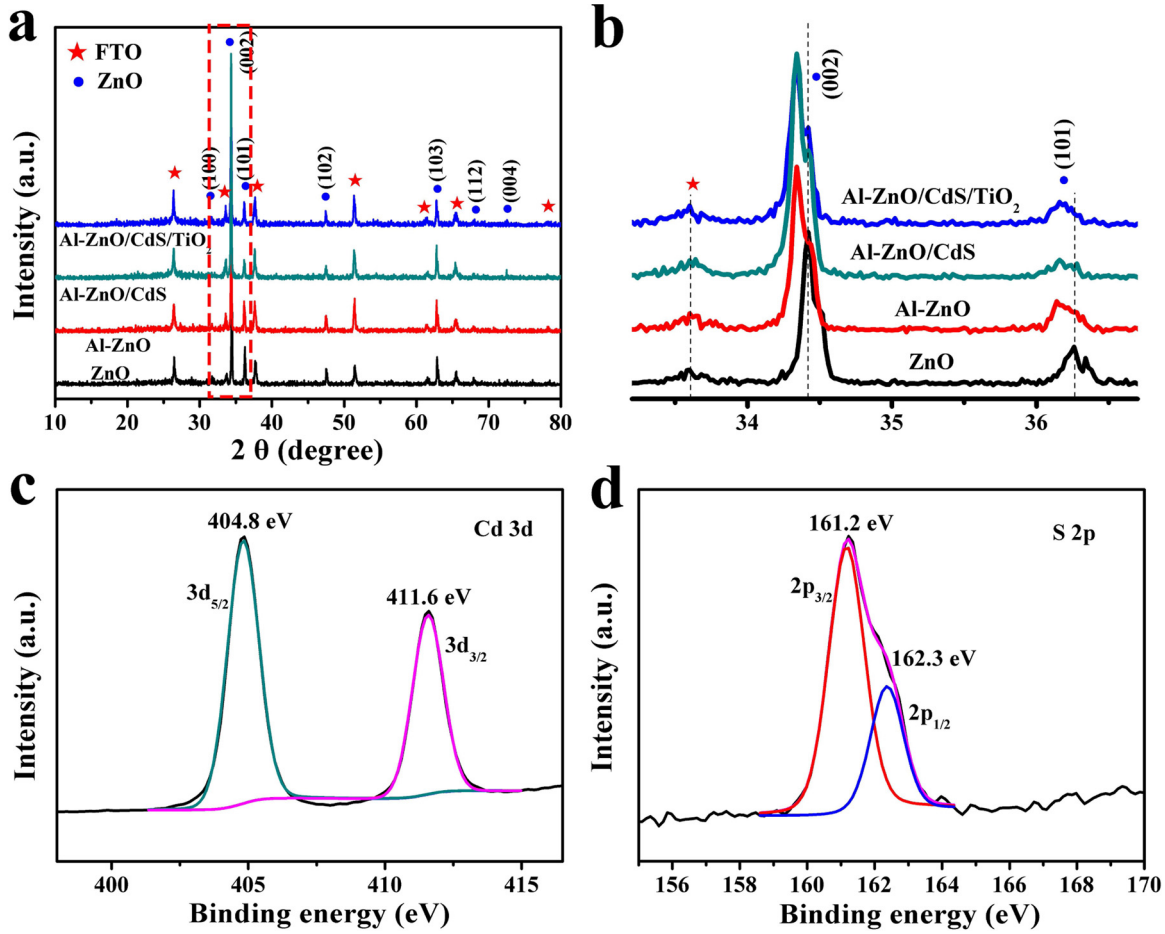

Fig. 2. (a) XRD patterns of the ZnO, Al-ZnO, Al-ZnO/CdS and Al-ZnO/CdS/TiO_2, (b) local enlarged in (a). XPS spectra of Al-ZnO/CdS (c) Cd 3d and (d) S 2p.

electrolyte [30,35].

In this work, atomic layer deposition (ALD) was used to deposit protective TiO_2 layer onto Al-ZnO/CdS photoanodes as schematically illustrated in Fig. 1. The Al-doping ZnO NRs array was first synthesized on FTO substrates. CdS nanoparticles were subsequently deposited onto ZnO NRs via a successive ionic layer adsorption reaction (SILAR) method. With this configuration, an efficient Al-ZnO/CdS/TiO_2 photoanode with a superior photostability was achieved. The mechanism of the charge separation and transmission with different thickness of TiO_2 is systematically studied.

2. Experimental section

2.1. Synthesis of Al-ZnO/CdS NRs

Al-ZnO/CdS NRs were prepared using a previously reported method [36]. The successive ionic layer adsorption reaction (SILAR) process for deposition CdS was repeated for 60 times. Then, a two-step low-temperature thermal treatment was then conducted at a muffle furnace to anneal the Al-ZnO/CdS NRs photoelectrodes at 150 °C for 10 min and then at 250 °C for another 10 min [37].

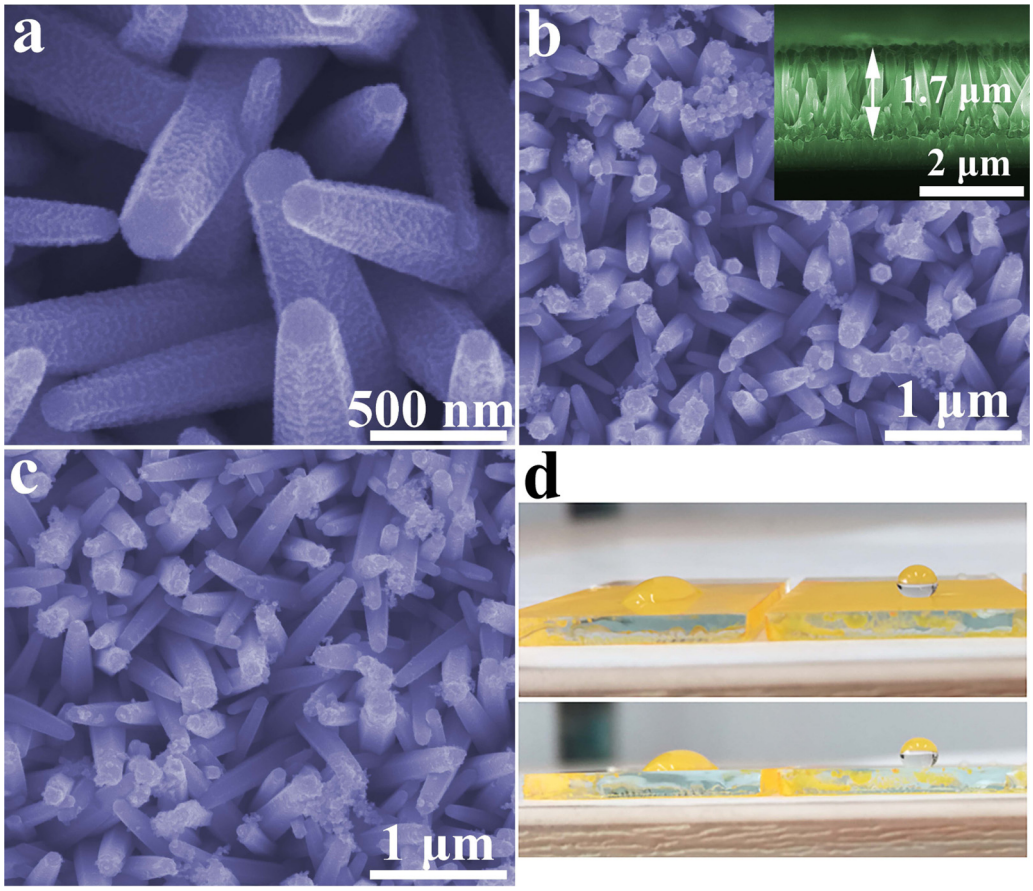

Fig. 3. SEM images of (a) Al-ZnO, inset shows a high magnification view, (b) Al-ZnO/CdS, inset are cross-sectional views, (c) Al-ZnO/CdS/TiO_2, (d) Photographs of a water droplet placed on Al-ZnO/CdS electrode (left) and Al-ZnO/CdS/TiO2 electrode (right).

2.2. ALD of TiO_2

ALD of TiO_2 was performed in an ALD reactor (Picosun SUNALETM R-150B), in which pulsed chemical precursors of titanium tetrachloride (Ti precursor) and deionized water (oxygen precursor) were supplied alternately in a N_2 carrier gas at 150 °C. The ALD cycles were repeated by 30, 60 and 150 times.

2.3. Characterization

The morphologies of samples were examined with a scanning electron microscope (SEM, Nova NanoSEM 230 FEI Co) and a transmission electron microscope (TEM, FEI Tecnai G2 F30 S-Twin, Hillsboro, OR). The crystal structures of the films were measured by X-ray diffraction (XRD, Rigaku Ultima III, Cu Kα radiation). The binding energy was investigated using X-ray photoelectron spectroscopy (XPS, Thermo ESCALAB 250). The binding energy was calibrated by C1s (284.6 eV). The UV-vis absorption spectra were obtained by a UV-vis spectrophotometer (UV-2550, Shimadzu).

2.4. Photoelectrochemical and electrochemical measurement

Photoelectrochemical properties were measured in a three-electrode cell using an electrochemical analyzer (CHI-660E, Shanghai Chenhua). An aqueous solution containing 0.25 M Na_2S and 0.35 M Na_2SO_3 (PH = 12.5) was employed as an electrolyte. An AM1.5 G sunlight simulator (100 mW cm^2, oriel 92251A-1000) was used as a light source for measurements. A sample we prepared, a Pt sheet and a saturated Ag/AgCl electrode were used as a working electrode, a counter electrode and a reference electrode, respectively. Potentials of the working electrode were shifted at a RHE (reversible hydrogen potential) scale by the formula $V_{RHE} = V_{Ag/AgCl} + V_0 + 0.05916 \times pH$, where V_{RHE} was the potential vs. a reversible hydrogen potential, $V_{Ag/AgCl}$ was the potential vs. Ag/AgCl electrode, $V_0 = 0.1976$ V at 25 °C and pH was the pH value of electrolyte. The film area exposed to the light was 0.28 cm^2. The conversion efficiency (η) is calculated from the LSV curve of the photoelectrode,

$$\eta\,(\%) = \left(\frac{J_p \times (1.23 - V)}{P_{light}} \times 100\%\right)$$

where J_p is the photocurrent density (mA/cm^2), V_{bias} is the bias applied between the working electrode and counter electrode, P_{light} is the power density of the incident light. Electrochemical impedance spectra (EIS) of samples were measured under illumination at the bias of the open-circuit voltages, respectively, in three electrode configuration and the frequencies between 0.1 Hz and 100 kHz.

3. Results and Discussion

3.1. Structure and morphology

Fig. 2**a** shows the XRD patterns of the as-prepared ZnO, Al-ZnO, Al-ZnO/CdS and Al-ZnO/CdS/TiO_2 photoanodes. The ultrahigh spike at 34.4°, corresponding to ZnO (002) planes, indicates the ZnO NRs are highly c-axis oriented [18]. After doping of Al ions, no additional diffraction peaks relating to Al appears. This is possibly attributed to that Al ions are likely to be presented in the interstitial sites due to small ionic radii (0.054 nm) with respect to Zn ions (0.074 nm) [36–38]. Deriving from the lattice expansion caused by doping of Al ions, the diffraction peaks of ZnO were shifted toward low angle obviously

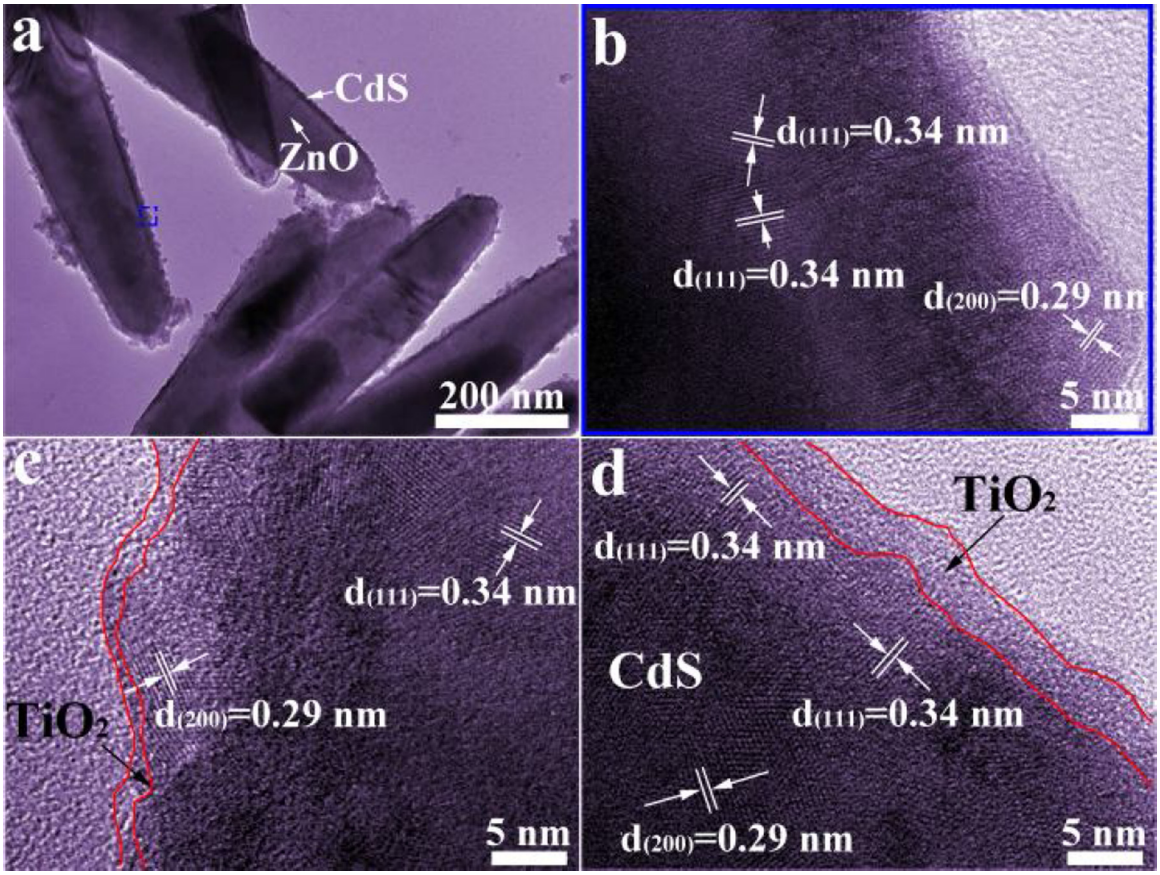

Fig. 4. (a) TEM and (b) HRTEM images of Al-ZnO/CdS, Al-ZnO/CdS coating with ALD TiO_2 with various cycles: (c) 30 cycles and (d) 60cycles.

(Fig. 2b). After SILAR deposition of CdS, there are no typical diffraction peaks of CdS on the pattern due to its relatively small particle size and polycrystallinity. However, the colour of the sample decided changed from gray to orange after composite CdS (**Fig. S1**). The results of XPS further prove the existence of CdS (**Fig. S2**). The high-resolution spectrum of Cd 3d in Fig. 2**c** with featured peaks of $3d_{5/2}$ at 404.9 eV and $3d_{3/2}$ at 411.6 eV indicates the +2 oxidation state (Cd^{2+}) in as prepared Al-ZnO/CdS photoanode [23]. The S 2p peaks at 161.2 eV and 162.3 eV are ascribed to S^{2-} in the CdS (**Fig. 2d**) [23,39].

Fig. 3**a** displays the top view SEM image of the Al-ZnO NRs, which are hexagonally and uniformly distributed on the FTO substrate with about 250 nm in diameter. Compared with undoped ZnO NRs (**Fig. S3**), the Al-ZnO possesses a rough surface, which favors for SILAR process for Cd^{2+} and S^{2-} ion adsorption to growth of the CdS coating layer [36]. After SILAR deposition, CdS nanoparticles can be clearly seen on the surface and top of the ZnO nanorods (Fig. 3b). The SEM image (Fig. 3c) and XRD study of ALD TiO_2 protective Al-ZnO/CdS electrode do not show noticeable change from those of untreated Al-ZnO/CdS. The first indication of TiO_2 coated was observed when a drop of water was placed on the surface of these electrodes to compare their hydrophilicities (Fig. 3d). While the Al-ZnO/CdS sample showed a high affinity to water, the TiO_2 coated sample showed strong hydrophobicity, which can considerably change the hydrophilicity of the surface. More importantly, this hydrophobic protective layer is beneficial in sequestering the direct interaction of CdS with O_2 and H_2O from the electrolyte solution, thus considerably retarding the photocorrosion of CdS upon light exposure [40].

The TiO_2 layer deposited on Al-ZnO/CdS by ALD was further investigated by high-resolution transmission electronic microscopy (HR-TEM). Fig. 4**a** shows the TEM image of the Al-ZnO/CdS, which presents the ZnO NRs is uniformly coated by a thin CdS layer. In Fig. 4b, the lattice spacing of 0.34 and 0.29 nm in the CdS layer correspond to (111) and (200) planes [21,41]. The Fig. 4**c** and **d** show the HR-TEM images of Al-ZnO/CdS NRs coated with TiO_2 layer deposited for 30 and 60 ALD cycles. It can be observed that an ultrathin amorphous TiO_2 layer (about 1.5 and 3 nm thick) was coated completely and uniformly on the Al-ZnO/CdS NRs.

3.2. Photoelectrochemical properties

Fig. 5**a** shows the comparison linear sweep voltammagram (LSV) curves of the pristine Al-ZnO/CdS and Al-ZnO/CdS/TiO_2 with different ALD cycles both in dark and under light illumination. All the photoanodes show very small photocurrent density in the dark, while under light illumination, obvious photocurrent density are observed, suggesting efficient light harvesting and charge separation at the photoanode/electrolyte interface. Compared with the pristine Al-ZnO, the photocurrent of the photoanode after deposition CdS has been boosting enhanced (**Fig. S4a**). This mainly attributed to the narrow band gap CdS extending the response range to visible light (**Fig. S4b**). The heterojunction between Al-ZnO and CdS could generate an interface electric field by band-edge offset, which can effectively accelerate the separation and transfer of photogenerated carriers **(Figure S5**). It is found that the photocurrent density increases with adding ALD cycles and reaches the maximum value at 30 cycles. When the ALD increases to 60 cycles, it reduces to 11.7 mA/cm^2 from 12.7 mA/cm^2 at 1.23 V versus RHE for the 30 cycles. When adds to 150 cycles, it further reduces to 9.2 mA/cm^2 even lower than the pristine Al-ZnO/CdS (10.4 mA/cm^2). The corresponding transient photocurrent density time (I-t) curves of all photoelectrodes were collected under chopped light illumination at 0 V versus Ag/AgCl, as displayed in Fig. 5**b**. All electrodes exhibit fast photoresponse and excellent photoswiching properties during light illumination on/off cycles. The current densities are 11.0 mA/cm^2, 11.9 mA/cm^2 and 10.8 mA/cm^2 for ALD 15, 30 and 60

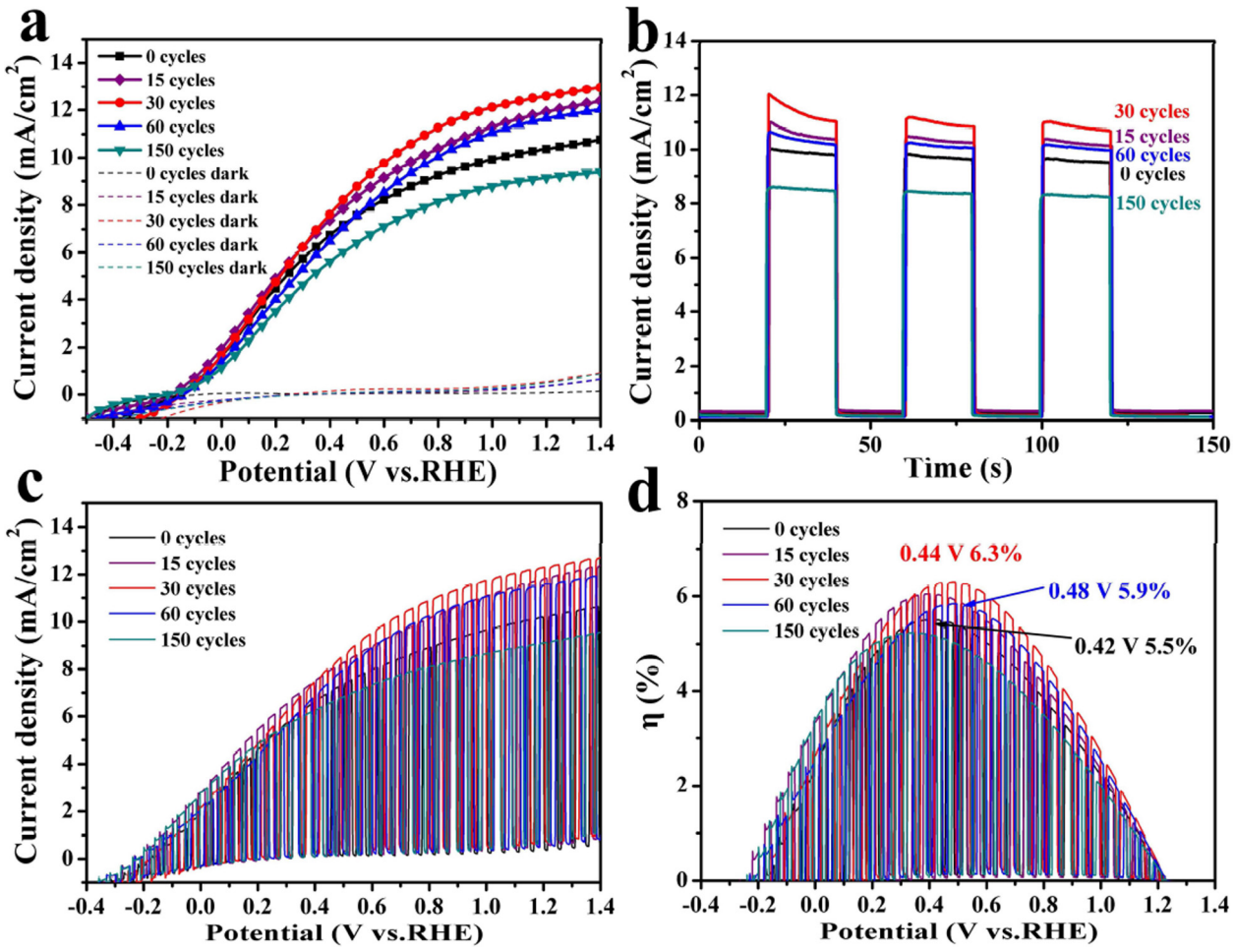

Fig. 5. (a) Linear sweep voltammograms of Al-ZnO/CdS coating with ALD TiO_2 with various cycles and (b) the corresponding amperometric I-t curves plotted at an external potential of 0 V versus Ag/AgCl, under chopped illumination. (c) Chopped illumination (100 mW/cm^2) current-voltage (I-V) characteristics of Al-ZnO/CdS coating with ALD TiO_2 with various cycles and (d) the corresponding photoconversion efficiencies calculated from I-V curves.

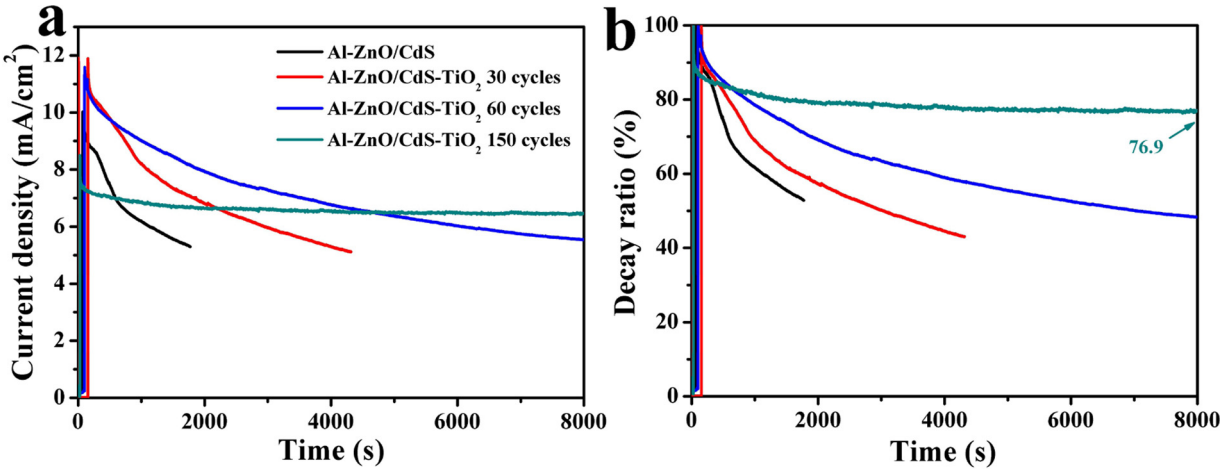

Fig. 6. (a) Stability measurements and (b) decay rate for Al-ZnO/CdS coating with 0, 30, 60 and 150 ALD TiO_2 cycles under illumination (100 mW/cm^2 with AM 1.5 G).

cycles, consistent with the values obtained from the LSV curves. To further investigate the charge generation/decay phenomenon kinetically, the light on/off experiment was performed (Fig. 5c). Both photoanodes show a fast and reproducible photoresponse per each cycle, and their quantitative value is identical to that of LSV. Conversion efficiency calculated from the chopped-light curves as shown in Fig. 5**d** reveals that the addition of dark current can be ignored. A conversion efficiency of 6.3 % was achieved at 0.44 V versus RHE for 30 ALD cycles. When ALD cycles adding to 60, it still has a conversion efficiency up to 5.9 %.

In addition to possess high current and conversion, long-term stability is another important challenge for the application of practical

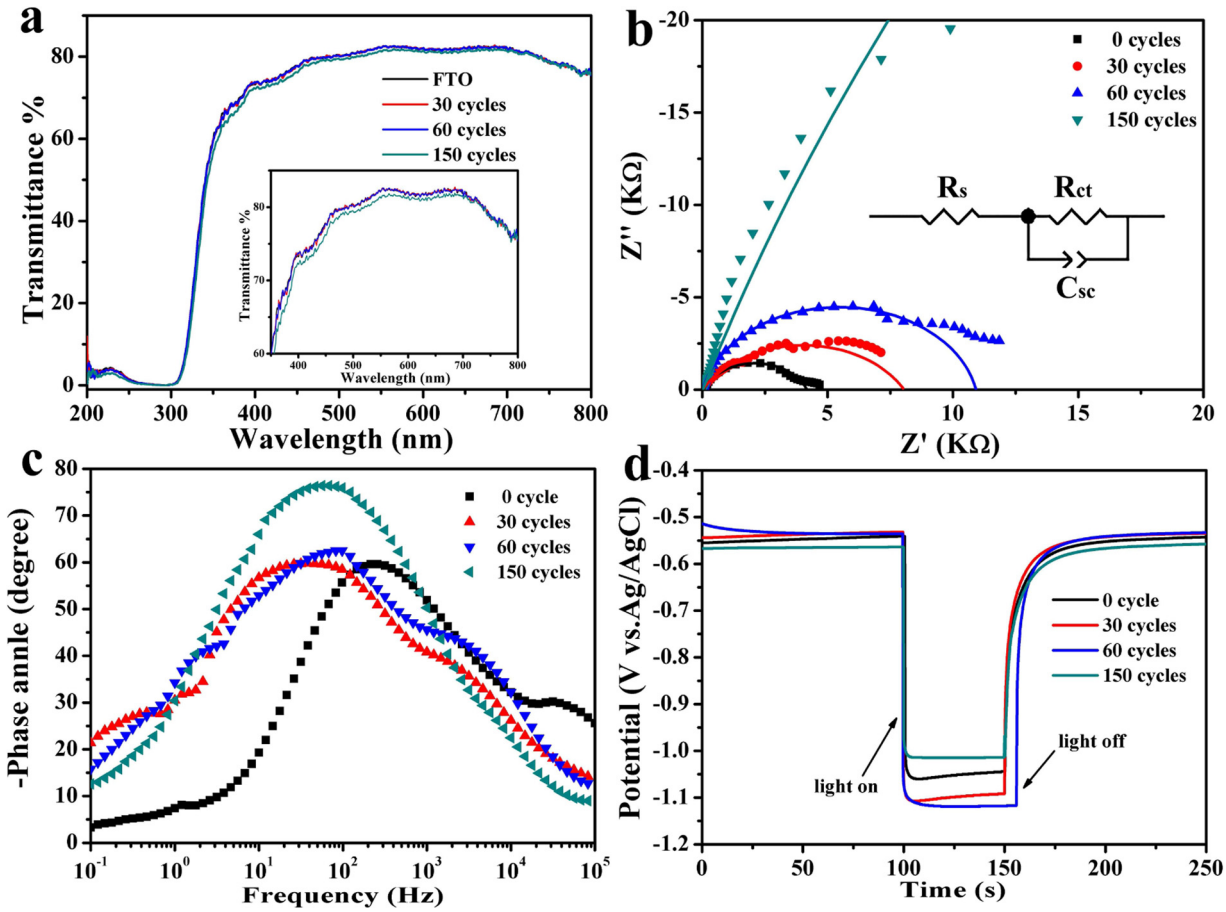

Fig. 7. (a) Transmittance spectra of Al-ZnO/CdS coating with ALD TiO_2 with various cycles, inset shows partial enlarged view. EIS spectra of Al-ZnO/CdS coating with ALD TiO_2 with various cycles (b) Nyquist plots and (c) Bode phase plots. (d) Open-circuit voltage decay (OCVD) curves measured for Al-ZnO/CdS coating with different cycles of ALD TiO_2.

PEC. The photostability was identified by measuring the photocurrent under continuous light illumination at 0 V versus Ag/AgCl. The unprotected pristine Al-ZnO/CdS electrode displays a continuous decrease of photocurrent. Since ALD 15 cycles of TiO_2 does not completely cover the Al-ZnO/CdS, only the samples with more than 30 cycles were explored (**Figure S6**). As shown in Fig. 6a, with the increasing of ALD cycles, the photostability of photoanodes are extended. To draw a further comparison, all the plots were converted into decay ratio versus time. As displayed in Fig. 6b, the photocurrent density of the pristine Al-ZnO/CdS has decayed to 52.6 % after 1800s illumination. Taking this value as the reference standard, the lifetime of 30 and 60 ALD cycles electeodes are 2700 and 6050 s, the photostability increases by approximate 1.5 and 3.4 times, respectively. It is further confirmed that the photostability has been significantly improved. The electrode of ALD TiO_2 for 150 cycles exhibits a photocurrent over 6.5 mA/cm^2 and remains 76.9% of the initial photocurrent after 8000 s continuous illumination. Photostability of ZnO/CdS based systems without co-catalysis at such high level of photocurrent within 2 hours has been barely achieved. (**Table S1**)

3.3. Mechanism and discussion

The PEC process involves three reaction steps: the generation of electron-hole pairs by absorbed photons, the separation and migration of charges to the electrode interface, and the surface water oxidation/reduction reaction with holes/electrons [42,43]. Achieving a large photocurrent and an efficient conversion indicate that all these sequential steps are achieved smoothly, which requires the electrode materials to simultaneously satisfy multiple requirements. As ALD TiO_2 has no effect on improving surface reaction kinetics, its impact on our system mainly concentrated in the former two processes.

Firstly, the transmittance of the TiO_2 layer was discussed as introducing a broadband gap protective layer may hinder the light absorption of the photoanode and reduce the photoelectric response. Fig. 7**a** shows the UV-vis transmittance of the ALD TiO_2 with different cycles. Compared with the bare FTO substrate, the optical absorption of the photoanode was not affected except for the 150 cycles with a slight reduction. This indicates when the number of the ALD cycles is less than 60, the TiO_2 protective layer has no effect on the photo absorption of the Al-ZnO/CdS, and its improvement in conversion efficiency is mainly focused on the separation and transfer of charges, as the following analysis.

With the ALD cycles more than 30, the photocurrent decreases gradually with increases cycles but has a better stability. This indicates that the TiO_2 layer is not only capable of promoting charge separation but also facilitating charge transmission to maintain a long period of photocurrent output. **Figure S7** shows the steady-state photoluminescence spectra of the samples. For the pristine Al-ZnO/CdS, the spectrum displays a strong emission peak at 650 nm. The intensity of this peak quenches remarkably after deposition TiO_2 by ALD, indicating acceleration of the separation of photogenerated carriers. EIS was measured to investigate the charge transfer properties of the samples. Fig. 7**b** shows Nyquist plots of all the samples, where symbols and solid lines represent experimental data and fitting results of these data to an equivalent Randles-Ershler circuit model (Fig. 7**b** inset). Here, Rs is series resistance, and Rct correspond to the charge transfer resistance across the interface. It can be seen that the arc radius of the EIS spectrum of the Al-ZnO/CdS/TiO_2 is larger than that of the Al-ZnO/CdS.

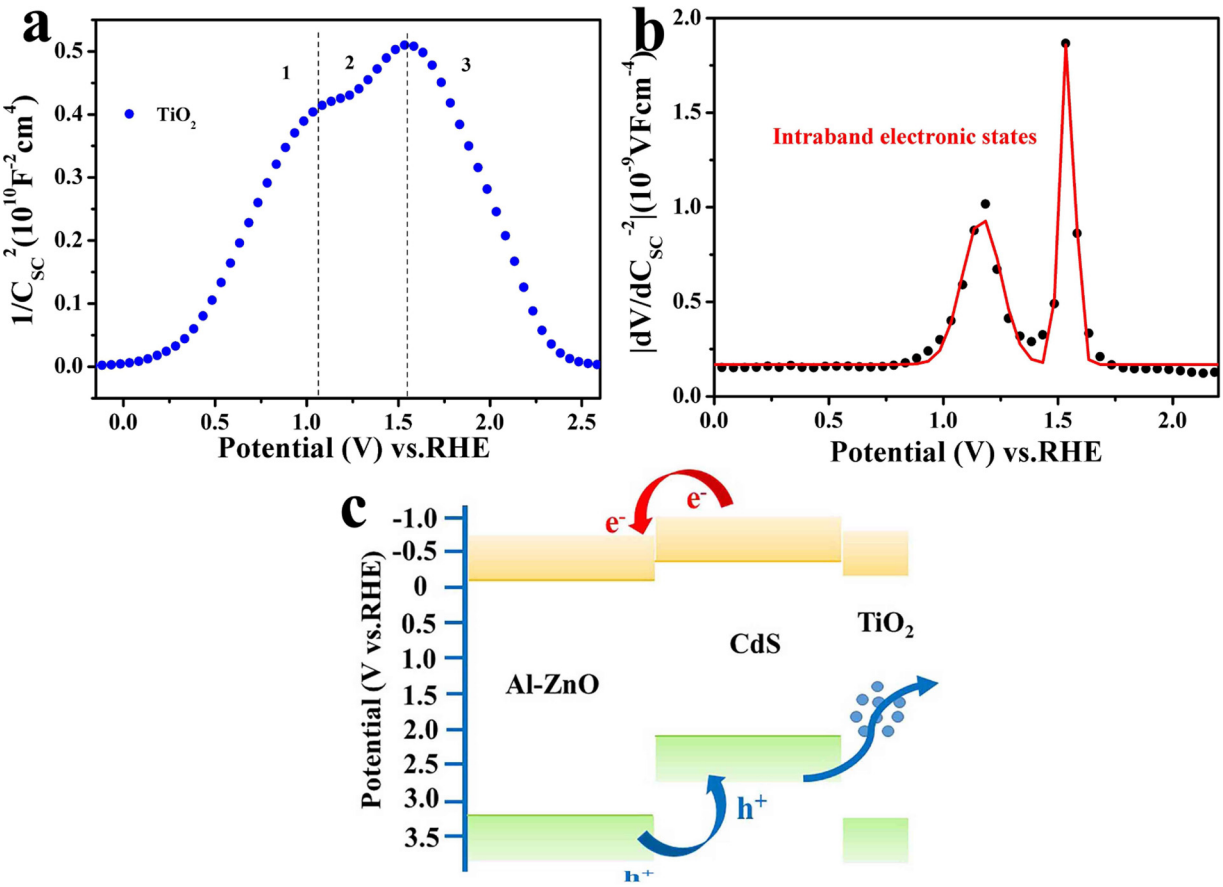

Fig. 8. (a) Mott-Schottky (MS) plot of the TiO_2/FTO electrode in 1 M NaOH aqueous solution with the AC potential frequency of 1000 HZ, (b) values taken from the derivative of the nonlinear MS plot of TiO_2/FTO, (c) band positions of Al-ZnO, CdS and TiO_2.

After TiO_2 was deposited on the surface, the charge transfer resistance increased significantly compared with the Al-ZnO/CdS photoanode (4125 Ω) (**Figure S8**). The diameter of the Nyquist plot at high frequency is correlated with the charge transfer process, reflecting the charge transfer resistance at the electrode/electrolyte interface [12,40]. The arc radius of the EIS spectrum of the Al-ZnO/CdS/TiO_2 is larger than that of the Al-ZnO/CdS. The enlarged impedance attribution to TiO_2 has lower electron mobility than that of ZnO [21]. In addition, the arc diameter increases with the increasing number of ALD from 30 to 150 cycles. This correlates well with the decrease of photocurrent density with the increased cycles of TiO_2. The electron lifetime (τ_n) is correlated with the frequency peak in Bode phase plots, $\tau_n = 1/(2\pi f_{max})$ [30,44]. As shown in Fig. 7c, the frequency value slightly decreases after coating TiO_2 protective layer, which means a longer electron lifetime. This suggests that the deposition of TiO_2 protection layer is more beneficial for the charge separation [44,45]. This can be further demonstrated by the open circuit voltage decay (OCVD) testing as shown in Fig. 7**d**. The equilibrium between electron accumulation and loss is established when constant illumination under open circuit. A more negative potential was obtained after coating TiO_2 protection layer, indicating a better charge separation and electron accumulation in the metal-semiconductor [43]. While for too thick protective layer (**Fig. S9**), it may increase the probability of electron hole recombination as for 150 ALD TiO_2 cycles have a more positive OCP. It seems that the protective TiO_2 layer is favorable for charge separation but not conducive for charge transfer, as has a larger impedance. However, we did get a better photoelectric response, especially for 150 cycles ALD TiO_2 electrode, a more stable photocurrent was obtained.

To explain the mechanism in it, the Mott-Schottky analysis of TiO_2 layer with 150 ALD cycles on FTO substrate was performed as shown in Fig. 8a, which is distinguish from that of bare FTO substrate (**Fig. S10**). The curve can be divided into three sections according to the different variations of capacitance versus potential. Section 1 exhibits a positive slope, which is a typical feature for an n-type semiconductor. In section 2, a stabilized capacitance is presented, associating with the surface redox states charging [46–48]. Remarkably, the energy levels of the electronic states can be obtained from the derivative of the Mott-Schottky plot [10,46], provided in Fig. 8**b**. The electronic states localized at 1.2 V and 1.6 V, which are above the valence band of TiO_2, might benefit to mediate hole transport from photoanode to electrolyte (Fig. 8c). This multiple electronic states can be confirmed from the results of the XPS (**Fig. S11**). The Ti $2p_{3/2}$ and Ti $2p_{1/2}$ peaks are centered at a binding energy of 464.2 eV and 458.3 eV, falling between the binding energies of Ti^{4+} and Ti^{3+} [49,50]. After the PEC testing, no significant change was observed in the valence state of Ti (**Fig. S12**), which may be related to the amorphous nature of TiO_2 [51], consistent with the observation in the HR-TEM image (**Fig. S9**). In section 3, a linear dependence with a negative slope reflects that a positively charged inversion layer is formed after these surface states are emptied, indicating that holes might be stored [48]. In this way, a higher and more stable photoelectric response obtained after ALD deposition can be well understood. In addition to passivate the surface state to reduce the probability of electron-hole recombiantion, the photogenerated holes of CdS can be captured and stored by protective TiO_2 layer, whilst blocking electron migration to the electrolyte. The photocorrosion is reduced, and the effective separation of charge is realized.

4. Conclusions

A highly efficient Al-ZnO/CdS/TiO_2 photoanode system was

demonstrated. Deriving from the high electron transport of the Al doped ZnO nanorod array, the appropriate bandgap of CdS absorption photon and TiO_2 serving as passivation layer, a high efficiency photoanode system was achieved. More impressively, the lifetime of Al-ZnO/CdS photoanode was extensive prolonged after ALD TiO_2 protective layer. The strengthen photostability is benefited from the triple functions of ALD TiO_2 layer, that is, isolating the direct contact between the photoanode and the surrounding liquid environment, passivating the surface state of the CdS, capturing and storing the photogenerated hole. Our work put forward a photoanode system with high conversion efficiency and superior photostability.

Conflict of interest

The authors declare no competing financial interest.

Acknowledgements

This work was supported by NSF of China (No. 21473091 and 21773114), NSF of Jiangsu Province (No. BK20171246), and Fundamental Research Funds for the Central Universities (No. 14380135).

Appendix A. Supplementary data

Supplementary material related to this article can be found, in the online version, at doi:https://doi.org/10.1016/j.apcatb.2019.05.040.

References

[1] Y.H. Yu, Z. Zhang, X. Yin, A. Kvit, Q.L. Liao, Z. Kang, X.Q. Yan, Y. Zhang, X.D. Wang, Enhanced photoelectrochemical efficiency and stability using a conformal TiO_2 film a black silicon photoanode, Nature Energy 2 (2017) 17045.
[2] C.R. Jiang, S.J.A. Moniz, H.A.Q. Wang, T. Zhang, J.W. Tang, Photoelectrochemical devices for solar water splitting-materials and challenges, Chem. Soc. Rev 46 (2017) 4645–4660.
[3] G.M. Carroll, D.K. Zhong, D.R. Gamelin, Mechanisitic insights into solar water oxidation by cobalt-phosphate-modified α–Fe_2O_3 photoanodes, Energy Environ. Sci 8 (2015) 577–584.
[4] L.M. Zhang, X.F. Ye, M. Boloor, A. Poletayev, N.A. Melosh, W.C. Chueh, Significantly enhanced photocurrent for water oxidation in monolithic Mo:$BiVO_4$/SnO_2/Si by thermally increasing the minority carrier diffusion length, Energy Environ. Sci. 9 (2016) 2044–2052.
[5] D.K. Lee, K.-S. Choi, Enhancing long-term photostability of $BiVO_4$ photoanodes for solar water splitting by tuning electrolyte composition, Nature Energy 3 (2018) 53–60.
[6] Y.B. Kuang, Q.X. Jia, G.J. Ma, T. Hisatomi, T. Minegishi, H. Nishiyama, M. Nakabayashi, N. Shibata, T. Yanmada, A. kudo, K. Domen, Ulreastable low-bias water splitting photoanodes via photocorrosion inhibition and *in situ* catalyst regeneration, Nature Energy 2 (2015) 1500049.
[7] Y. Wu, H. Wang, W.G. Tu, S.Y. Wu, Y. Liu, Y.Z. Tan, H.J. Luo, X.Z. Yuan, J.W. Chew, Petal-like CdS nanostructures coated with exfoliated sulfur-doped carbon nitride via chemically activated chain termination for enhanced visible-light-driven photocatalytic water purification and H_2 generation, Appl. Catal. B Environ. 229 (2018) 181–191.
[8] J.Y. Zhang, Y.H. Wang, J. Jin, J. Zhang, Z. Lin, F. Huang, J.G. Yu, Efficient visible-light photocatalytic hydrogen evolution and enhanced photostability of core/shell CdS/g-C_3N_4 nanowires, ACS Appl. Mater. Interfaces 5 (2013) 10317–10324.
[9] D.L. Peng, H.H. Wang, K. Yu, Y. Chang, X.G. Ma, S.J. Dong, Photochemical preparation of the ternary composite CdS/Au/g-C_3N_4 with enhanced visible light photocatalytic performance and its microstructure, RSC Adv. 6 (2016) 77760–77767.
[10] X.F. Cui, Y.J. Wang, G.Y. Jiang, Z. Zhao, C.M. Xu, A.J. Duan, J. Liu, Y.C. Wei, W.K. Bai, The encapsulation of CdS in carbon nanotubes for stable and efficient photocatalysis, J. Mater. Chem. A 2 (2014) 20939–20946.
[11] L. Liu, H.L. Hou, L. Wang, R. Xu, Y. Lei, S.H. Shen, D.J. Yang, W.Y. Yang, A transparent CdS@TiO_2 nanotextile photoanode with boosted photoelectrocatalytic efficiency and stability, Nanoscale 9 (2017) 15650–15657.
[12] Z.C. Lian, P.P. Xu, W.C. Wang, D.Q. Zhang, S.N. Xiao, X. Li, G.S. Li, C_{60}-decorated CdS/TiO_2 mesoporous architectures with enhanced photostability and photocatalytic activity for H_2 evolution, ACS Appl. Mater. Interfaces 7 (2015) 4533–4540.
[13] J.P. Song, P.F. Yin, J. Mao, S.Z. Qiao, X.W. Du, Catalytically active and chemically inert $CdIn_2S_4$ coating on a CdS photoanode for efficient and stable water splitting, Nanoscale 9 (2017) 6296–6301.
[14] K. Zhao, X.Q. Yan, Y.S. Gu, Z. Kang, Z.M. Bai, S.Y. Cao, Y.C. Liu, X.H. Zhang, Y. Zhang, Self-powered photoelectrochemical biosensor based on CdS/RGO/ZnO nanowire array heterostructure, Small 12 (2016) 245–251.
[15] C.M. Li, T.H. Ahmed, M.G. Ma, T. Edvinsson, J.F. Zhu, A facile approach to ZnO/CdS nanoarrays and their photocatalytic and photoelectrochemical properties, Appl. Catal. B Environ. 17 (2013) 175–183.
[16] W.W. Zhang, W.Z. Wang, H.L. Shi, Y.J. Liang, J.L. Fu, M. Zhu, Surface plasmon-driven photoelectrochemical water splitting of aligned ZnO nanorod arrays decorated with loading-controllable Au nanoparticles, Sol. Energy Mater. and Sol. Cells 180 (2018) 25–33.
[17] Y.W. Choi, M.K. Beak, Z. Zhang, V.D. Dao, H.S. Choi, K.J. Yong, A two-storey structured photoanode of a 3D Cu_2ZnSnS_4/CdS/ZnO@steel composite nanostructure for efficient photoelectrochemical hydrogen generation, Nanoscale 7 (2015) 15291–15299.
[18] C.X. Guo, J.L. Xie, H.B. Yang, C.M. Li, Au@CdS core-shell nanoparticles-modified ZnO nanowires photoanode for efficient photoelectrochemical water splitting, Adv. Sci. 2 (2015) 1500135.
[19] Z.M. Yuan, L.W. Yin, CdSe-CdS quantum dots co-sensitized ZnO hierarchical hybrids for solar cells with enhanced photo-electrical conversion efficiency, Nanoscale 6 (2014) 13135–13144.
[20] H.J. Li, Y. Zhou, L. Chen, W.J. Luo, Q.F. Xu, X.Y. Wang, M. Xiao, Z.G. Zou, Rational and scalable fabrication of high-quality WO_3/CdS core/shell nanowire arrays for photoanodes toward enhanced charge separation and transport under visible light, Nanoscale 5 (2013) 11933–11939.
[21] Z.M. Bai, X.Q. Yan, Y. Li, Z. Kang, S.Y. Cao, Y. Zhang, 3D-branched ZnO/CdS nanowire arrays for solar water splitting and the service safety research, Adv. Energy Mater 6 (2016) 1501459.
[22] S.Y. Cao, X.Q. Yan, Z. Kang, Q. Liang, X.Q. Liao, Y. Zhang, Band alignment engineering for improved performance and stability of $ZnFe_2O_4$ modified CdS/ZnO nanostructured photoanode for PEC water splitting, Nano Energy 24 (2016) 25–31.
[23] P.Y. Kuang, Y.Z. Su, K. Xiao, Z.Q. Liu, N. Li, H.J. Wang, J. Zhang, Double-shelled CdS- and CdSe-cosensitized ZnO porous nanotube arrays for superior photoelectrocatalytic applications, ACS Appl. Mater.Interfaces 7 (2015) 16387–16394.
[24] M. Seol, J. Jang, S. Cho, J.S. Lee, K. Yong, Highly efficient and stable cadmium chalcogenide quantum dot/ZnO nanowires for photoelectrochemical hydrogen generation, Chem. Mater. 25 (2013) 184–189.
[25] M.R. Shaner, S. Hu, K. Sun, N.S. Lewis, Stabilization of Si microwire arrays for solar-driven H_2O oxidation to O_2 (g) in 1.0 M KOH (aq) using conformal coating of amorphous TiO_2, Energy Environ. Sci. 8 (2015) 203–207.
[26] H.D. She, Y.D. Sun, S.P. Li, J.W. Huang, L. Wang, G.Q. Zhu, Q.Z. Wang, Synthesis of non-noble metal nickel doped sulfide solid solution for improved photocatalytic performance, Appl. Catal. B Environ. 245 (2019) 439–447.
[27] Y.H. Ko, Y.C. Kim, S.Y. Kong, S.C. Kunnan, Y.S. Jun, Improved performance of sol-gel ZnO-based perovskite solar cells via $TiCl_4$ interfacial modification, Sol. Energy Mater. and Sol. Cells 183 (2018) 157–163.
[28] H.D. She, M. Jiang, P.F. Yue, J.W. Huang, L. Wang, J.Z. Li, G.Q. Zhu, Q.Z. Wang, Metal (Ni^{2+}/Co^{2+}) sulfides modified $BiVO_4$ for effective improvement in photoelectrochemical water splitting, J. Colloid and Inter. Sci. 549 (2019) 80–88.
[29] C.Y. Lee, H.S. Park, J.C. Fontecilla-Camps, E. Reisner, Photoelectrochemical H2 evolution with a hydrogenase immobilized on a TiO_2-protected silicon electrode, Angew. Chem. Int. Ed 55 (2016) 5971–5974.
[30] R. Liu, Z. Zhang, J. Spurgeon, X.G. Yang, Enhanced photoelectrochemical water-splitting performance of semiconductors by surface passivation layers, Energy Environ. Sci 7 (2014) 2504–2517.
[31] J. Qiu, G.T. Zeng, M.A. Ha, B.T. Hou, M. Mecklenburg, H.T. Shi, A.N. Alexandrova, S.B. Cronin, Microscopic study of atomic layer deposition of TiO_2 on GaAs and its photocatalytic application, Chem. Mater 27 (2015) 7977–7981.
[32] S. Hu, M.R. Shaner, J.A. Beardslee, M. Lichterman, B.S. Brunschwig, N.S. Lewis, Amorphous TiO_2 coating stabilize Si, GaAs, and GaP photoanodes for efficient water oxidation, Science 344 (2014) 1005–1009.
[33] J. Gu, Y. Yan, J.L. Young, K.X. Steirer, N.R. Neale, J.A. Turner, Water reduction by a p-$GaInP_2$ photoelectrode stabilized by an amorphous TiO_2 coating and a molecular cobalt catalyst, Nature Mater 15 (2016) 456–460.
[34] Y.W. Chen, J.D. Prange, S. Dühnen, Y. Park, M. Gunji, C.E.D. Chidsey, P.C. Mclntyre, Atomic layer-deposited tunnel oxide stabilizes silicon photoanodes for water oxidation, Nature Mater 10 (2011) 539–544.
[35] Z. Xie, X.X. Liu, W.P. Wang, X.J. Wang, C. Liu, Q. Xie, Z.C. Li, Z.J. Zhan, Enhanced photoelectrochemical and photocatalytic performance of TiO_2 nanorod arrays/CdS quantum dots by coating TiO_2 through atomic layer deposition, Nano Energy 11 (2015) 400–408.
[36] R.Y. Wang, X.D. Li, L. Wang, X.R. Zhao, G.C. Yang, A.D. Li, C.P. Wu, Q. Shen, Y. Zhou, Z.G. Zou, Construction of Al-ZnO/CdS photoanodes modified with distinctive alumina passivation layer for improvement of photoelectrochemical efficiency and stability, Nanoscale 10 (2018) 19621–19627.
[37] Q. Nie, L. Yang, C. Cao, Y.M. Zeng, G.Z. Wang, C.Z. Wang, S.W. Lin, Interface optimization of ZnO nanorod/CdS quantum dots heterostructure by a facile two-step low-temperature thermal treatment for improved photoelectrochemical water splitting, Chem. Eng. J 325 (2017) 151–159.
[38] T.V.L. Thejaswini, D. Prabhakaran, M.A. Maheswari, Soft synthesis of potassium co-doped Al-ZnO nanocomposites: a comprehensive study on their visible-light driven photocatalytic activity on dye degradation, J. Mater. Sci 51 (2016) 8187–8208.
[39] Y.C. Liu, Z. Kang, H.N. Si, P.F. Li, S.Y. Cao, S. Liu, Y. Li, S.C. Zhang, Z. Zhang, Q.L. Liao, L. Wang, Y. Zhang, Cactus-like hierarchical nanorod-nanosheet mixed dimensional photoanode for efficient and stable water splitting, Nano Energy 35 (2017) 189–198.
[40] M.Y. Wang, L.J. Cai, Y. Wang, F.C. Zhou, K. Xu, X.M. Tao, Y. Chai, Graphene-draped semiconductors for enhanced photocorrosion resistance and photocatalytic properties, J. Am. Chem. Soc. 139 (2017) 4144–4151.

[41] Y. Tak, H. Kim, D. Lee, K. Yong, Type-II CdS nanoparticle-ZnO nanowire heterostructure arrays fabricated by a solution process: enhanced photocatalytic activity, Chem. Commun. 38 (2008) 4585–4587.
[42] J. Yang, D. Wang, H. Han, C. Li, Roles of cocatalysts in photocatalysis and photoelectrocatalysis, Acc. Chem. Res 46 (2013) 1900–1909.
[43] T. Hisatomi, J. Kubota, K. Domen, Recent advances in semiconductors for photocatalytic and photoelectrochemical water splitting, Chem. Soc. Rev 43 (2014) 7520–7535.
[44] C.W. Cheng, S.K. Karuturi, L.J. Liu, J.P. Liu, H.X. Li, L.T. Su, A.L.Y. Tok, H.J. Fan, Quantum-dot-sensitized TiO_2 inverse opals for photoelectrochemical hydrogen generation, Small 8 (2012) 37–42.
[45] X. Liu, N. Chen, Y.X. Li, D.Y. Deng, X.X. Xing, Y.D. Wang, A general nonaqueous sol-gel route to g-C_3N_4 –coupling photocatalysts: the case of Z-scheme g-C_3N_4/TiO_2 with enhanced photodegradation toward RhB under visible-light, Sci. Rep. 6 (2016) 39531.
[46] M. Tomkiewicz, The potential distribution at the TiO_2 aqueous electrolyte interface, J. Electrochem. Soc. 126 (1979) 1505–1510.
[47] B. Klahr, S. Gimenez, F. Fabregat-Santiago, J. Bisquert, T.W. Hamann, Electrochemical and photoelectrochemical investigation of water oxidation with hematite electrodes, Energy Environ. Sci. 5 (2012) 7626–7636.
[48] G.J. Liu, J.Y. Shi, F.X. Zhang, Z. Chen, J.F. Han, C.M. Ding, S.S. Chen, Z.L. Wang, H.X. Han, C. Li, A tantalum nitride photoanode modified with a hole-storage layer for highly stable solar water splitting, Angew. Chem. Int. Ed. 53 (2014) 7295–7299.
[49] G.M. Wang, H.Y. Wang, Y.C. Ling, Y.C. Tang, X.Y. Yang, R.C. Fitzmorris, C.C. Wang, J.Z. Zhang, Y. Li, Hydrogen-treated TiO2 nanowire arrays for photoelectrochemical water splitting, Nano. Lett. 11 (2011) 3026–3033.
[50] H. Zhou, Y.R. Zhang, Electrochemically self-doped TiO_2 nanotube arrays for supercapacitors, J. Phys. Chem. C. 118 (2014) 5626–5636.
[51] G.J. Liu, S. Ye, P.L. Yan, F.Q. Xiong, P. Fu, Z.L. Wang, Z. Chen, J.Y. Shi, C. Li, Enabling an integrated tantalum nitride photoanode to approach the theoretical photocurrent limit for solar water splitting, Energy Environ. Sci. 9 (2016) 1327–1334.